

Entanglement enhanced estimation of parameter embedded in multiple phases

Michael R. Grace,¹ Christos N. Gagatsos,¹ and Saikat Guha¹

¹*James C. Wyant College of Optical Sciences, University of Arizona, Tucson, AZ 85721, USA*

Quantum enhanced sensing promises to improve the performance of sensing tasks using non-classical probes and measurements using far less scene-modulated photons than possible by the best classical scheme, thereby gaining previously-inaccessible quantitative information about a wide range of physical systems. We propose a generalized distributed sensing framework that uses an entangled quantum probe to estimate a scene-parameter that is encoded within an array of phases, with a functional dependence on that parameter determined by the physics of the actual system. The receiver uses a laser light source enhanced by quantum-entangled multi-partite squeezed-vacuum light to probe the phases, to estimate the desired scene parameter. The entanglement suppresses the collective quantum vacuum noise across the phase array. We show our approach enables Heisenberg limited sensitivity in estimating the scene parameter with respect to total probe energy, as well as with respect to the number of modulated phases, and saturates the quantum Cramér Rao bound. We apply our approach to examples as diverse as radio-frequency phased-array directional radar, fiber-based temperature gradiometer, and beam-displacement tracking for atomic-force microscopy.

Introduction—Quantum phenomena that enhance estimation precision are of paramount importance in diverse fields, e.g., astronomy [1], general relativity [2–5], models for quantum-to-classical transition [6], microscopy [7], optical imaging [8–10], and networked sensors [11, 12]. Quantum-enhanced estimation in sensing applications arguably comprises the nearest-term realizable quantum technologies of practical importance.

The added attraction of quantum estimation in photonic sensors stems from the fact that quantum enhanced performance in sensing can be obtained using *Gaussian* quantum states of light (which can be generated using lasers, linear optics, and squeezed light, e.g., produced using parametric amplifiers) and *Gaussian* measurements (i.e., homodyne and heterodyne detection). Gaussian states, unitary operations and measurements admit an elegant mathematical description [13, 14], which can be readily analyzed as well as realized experimentally [15, 16]. This is an especially interesting point, since Gaussian resources alone do *not* suffice to perform a variety of quantum information tasks, as described in various no-go theorems for: universal quantum computing [17], entanglement distillation of Gaussian states [18–20], optimal cloning of coherent states [21], optimal discrimination of coherent states [22, 23], Gaussian quantum error correction [24] and receivers to achieve the Holevo capacity for classical communications [25].

In this Letter, we consider the following scenario: a single scalar scene-parameter x modulates phases $\theta_m(x)$, $1 \leq m \leq M$ in an array of M Mach-Zehnder Interferometers (MZIs), each with two input modes and two output modes. Given a total mean photon number budget N , one is tasked with designing a $2M$ -mode (quantum) optical probe, and an associated receiver measurement, to minimize the variance of the estimate of x . There has been some recent concurrent work considering a similar scenario [26–28] [29]. This is a powerful scenario, which can be used to model various practical photonic sensing

problems. Some examples are: estimation of the angle of incidence of a radio-frequency (RF) wave upon an array of sensor pixels where each pixel is a phase modulator that is read out optically [30], estimation of a small angular velocity of rotation of a Sagnac-based fiber-optical gyroscope (FOG) [31], and estimating a small transverse displace of an optical beam in an atomic-force microscope (AFM) [32]. In the above examples, M , respectively would refer to: the number of sensor pixels of the RF photonic antenna, the number of fiber loops stacked together to build a FOG, and the number of orthogonal spatio-temporal modes in the probe’s time-bandwidth product and the free-space propagation geometry. In these examples, the scene parameter of interest x could refer to: the angle of incidence of the impinging RF field, the radians-per-second rotation experienced by the FOG, and the longitudinal displacement of a nano-cantilever of an AFM, respectively. Not only does our setting apply to the aforesaid three photonic sensors, it has applicability in several more, including a fiber-based temperature gradiometer, and a doppler vibrometer. Finally, applications of the theory we develop goes beyond photonic sensors, and could serve as foundation for more general distributed quantum sensing tasks with applications to quantum process tomography of photonic quantum computers, and quantum network tomography.

Problem setup—The two tools from estimation theory we use are the quantum Fisher information (QFI) H_x and the classical Fisher information (CFI) I_x , both of which give lower bounds to the mean squared error (MSE) $\langle(\hat{x} - x)^2\rangle$ for unbiased estimators \hat{x} (i.e., $\langle\hat{x}\rangle = x$), via the classical and quantum Cramér-Rao bounds: $\langle(\hat{x} - x)^2\rangle \geq I_x^{-1} \geq H_x^{-1}$. The QFI, a function of the quantum description ρ_x of the light modulated by the scene-parameter, quantifies the optimal precision achievable in estimating x by any receiver. The CFI quantifies the precision achievable by a specific receiver, but allowing for arbitrary post-processing. In the quantum

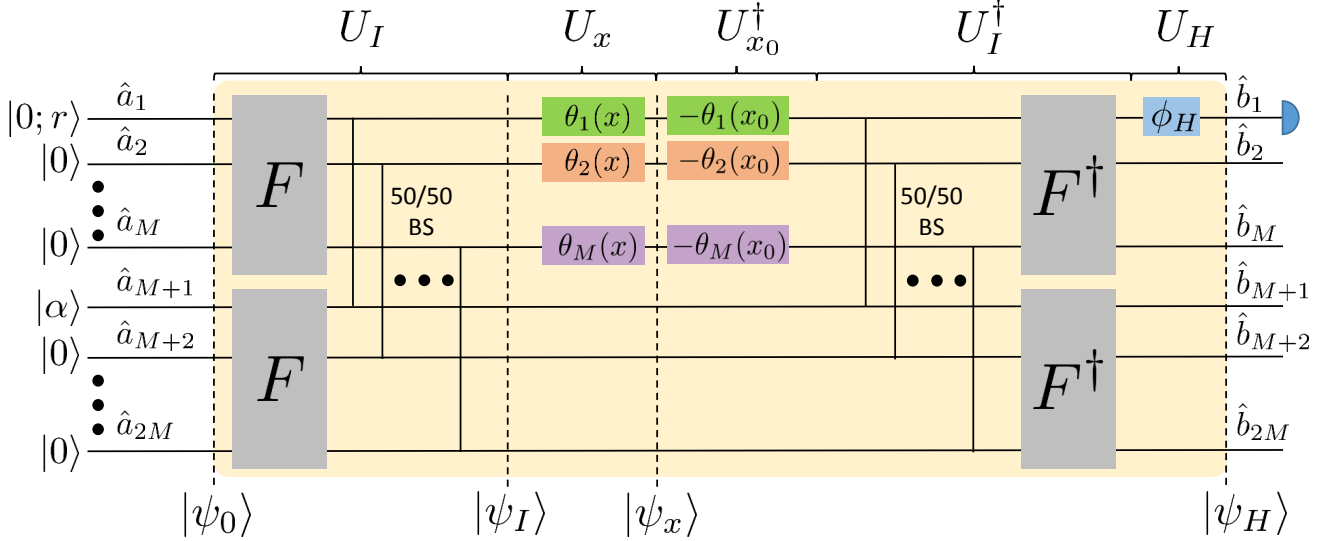


FIG. 1. Distributed sensing of a single parameter of interest x embedded in phase functions $\theta_m(x)$ modulating M MZIs. Each two-mode MZI is probed with a coherent state and one mode of an M -mode-entangled squeezed vacuum state. F , the Fourier gate, is an M -mode linear-optical interferometer, and the detector at the output of the circuit is a homodyne detector.

metrology literature [33], it has been shown for various settings that in the absence of loss and noise, quantum optical probes can attain the so-called Heisenberg scaling $H_x = O(N^2)$, where N is the total photon-unit energy in the probe field. In contrast, sensing using classical probes and measurements can only achieve $I_x = O(N)$ at best. If the CFI I_x for a specific quantum probe and a receiver scales as $O(N^2)$, that system design saturates the Heisenberg scaling limit.

The $2M$ -mode circuit shown in Fig. 1 depicts the system we describe above for probing the M phases $\theta_m(x)$, which is implementable using passive linear optics. Our probe consists of a single-mode squeezed vacuum (SV) $|0; \xi\rangle$ with mean photon number $N_s = \sinh^2(\xi)$ and a coherent state $|\alpha\rangle$ with mean photon number $N_v = |\alpha|^2$. Each of these two inputs are equally mixed with $M - 1$ vacuum modes on balanced “Fourier gates” F , and the outputs are fed into the $2M$ MZI ports. The output of the first Fourier gate is a multi-partite, continuous-variable (CV) entangled state exhibiting mutual quantum entanglement across M modes [12], while the output of the second Fourier gate is simply a coherent state split into M identical (product) coherent states, $|\alpha/\sqrt{M}\rangle$. The QFI H_x only depends on $\rho_x = |\psi_x\rangle\langle\psi_x|$, the pure state obtained immediately after the parameter-encoding phases are encountered. The receiver whose I_x we analyze is also shown, and involves application of phases $-\theta_m(x_0)$ to the M modulated modes, followed by a linear-optical circuit, and a single-mode homodyne detection receiver.

Quantum Fisher Information— We compute the QFI on x from the quantum fidelity between the state ρ_x and

$\rho_{x+\epsilon}$, defined as $\mathcal{F}(\rho_x, \rho_{x+\epsilon}) = \text{tr}\left((\rho_x^{1/2} \rho_{x+\epsilon} \rho_x^{1/2})^{1/2}\right)^2$, where ϵ is a vanishingly small number. The QFI $H_x = 4g(\rho_x)$ is related to the fidelity through the Bures metric $g(\rho_x)$ via $g(\rho_x)d^2x = 2(1 - \mathcal{F}(\rho_x, \rho_{x+\epsilon})^{1/2})$ [34], resulting in the relation

$$H_x = -2 \frac{\partial^2 \mathcal{F}(\rho_x, \rho_{x+\epsilon})}{d\epsilon^2} \Big|_{\epsilon \rightarrow 0}. \quad (1)$$

Since ρ_x is a pure state, i.e., $\rho_x = |\psi_x\rangle\langle\psi_x|$ with $|\psi_x\rangle = U_x U_I |\psi_0\rangle$, the fidelity $\mathcal{F}(\rho_x, \rho_{x+\epsilon}) = |\langle\psi_x|\psi_{x+\epsilon}\rangle|^2 = |\langle U_x^\dagger U_{x+\epsilon}\rangle_I|^2$, where the notation $\langle \cdot \rangle_I$ represents an expectation over the state $|\psi_I\rangle = U_I |\psi_0\rangle$. The unitary U_x is the application of phases $\theta_m(x)$ on the first M modes; $U_x = \exp\left(i \sum_{m=1}^M \theta_m(x) \hat{n}_m\right)$, where $\hat{n}_m = \hat{a}_m^\dagger \hat{a}_m$ is the number operator on the m^{th} mode. Applying Eq. 1, we can express the QFI as $H_x = 4 \langle \Delta \Lambda_x^2 \rangle_I$, in terms of the variance of $\Lambda_x = \sum_{m=1}^M (\partial \theta_m(x) / \partial x) \hat{n}_m$ with respect to $|\psi_I\rangle$. Expanding this variance, we get the following:

$$H_x = 4 \sum_{\{m,l\}=1}^M \frac{\partial \theta_m(x)}{\partial x} \frac{\partial \theta_l(x)}{\partial x} \left(\langle \hat{n}_m \hat{n}_l \rangle_I - \langle \hat{n}_m \rangle_I \langle \hat{n}_l \rangle_I \right). \quad (2)$$

This is our first main result: a general expression for the QFI of a single parameter embedded in phases $\theta_m(x)$ probed with a pure state $|\psi_I\rangle$. The M^2 summation elements in Eq. 2 each factor into contributions from derivatives of the phase functions and the moments of the number operators with respect to the probe state.

If $|\psi_I\rangle$ is a $2M$ -mode Gaussian state, as in Fig. 1, the moments of the number operators can be found from

the $4M$ quadrature means \vec{d}_I and the $4M \times 4M$ covariance matrix (CM) V_I . Our conventions are that the elements of mean vectors and CMs are indexed according to $\vec{r} = \{\vec{q}, \vec{p}\}$, where \vec{q} and \vec{p} are the $2M$ real and imaginary mode quadratures, and $\hbar \equiv 1$. The probe state quadrature means \vec{d}_0 and CM V_0 evolve through the unitary operation U_I according to $\vec{d}_I = S_I \vec{d}_0$ and $V_I = S_I V_0 S_I^T$, where S_I is a symplectic matrix defined as

$$S(x) = \begin{pmatrix} \text{Re}\{U_I\} & -\text{Im}\{U_I\} \\ \text{Im}\{U_I\} & \text{Re}\{U_I\} \end{pmatrix}, \quad (3)$$

and where $U_I = F_{M \times M} \otimes F_{2 \times 2}$ is a tensor product of Fourier gates. Calculating the moments in Eq. 2 from the Wigner function $W(\vec{r}) = (1/(2\pi)^2 M \sqrt{\det(V_I)}) \exp(-(\vec{r} - \vec{d}_I)^T V_I^{-1} (\vec{r} - \vec{d}_I))$ while obeying the canonical commutation relations $[q_m, p_m] = i$, we find the QFI to be

$$H_x = \langle \partial\theta(x) \rangle^2 \left[N_v (\sqrt{N_s} + \sqrt{N_s + 1})^2 + 2N_s(N_s + 1) - (N_v + N_s) \right] + 2 \langle \partial\theta^2(x) \rangle (N_v + N_s), \quad (4)$$

where $\langle \partial\theta(x) \rangle = (1/M) \sum_{m=1}^M \partial\theta_m(x) / \partial x$ and where $\langle \partial\theta^2(x) \rangle = (1/M) \sum_{m=1}^M (\partial\theta_m(x) / \partial x)^2$. By inspection, the first two terms of the QFI scale quadratically with energy as $N_v \gg 1$ and $N_s \gg 1$, the first of which depends on both input energy sources while the second only depends on the injected SV.

Classical Fisher Information of Proposed Receiver—Let us assume that the parameter x is known to be close to some value x_0 , i.e., $|x - x_0| \ll 1$, due to either *a priori* information or a preliminary estimate of x . When the M phases are an identical constant, i.e., $\theta_m(x) = cx, \forall m$, for some constant c , the optimal linear recombination of the phase-modulated modes prior to detection (using a single homodyne detection receiver) is the application of conjugate phases matched to the pre-estimate, $-\vec{\theta}(x_0)$, a sequence of 50-50 beamsplitters (i.e., the second beamsplitters of the MZIs) and inverse Fourier transforms as shown in Fig. 1 [31]. Application of $-\vec{\theta}(x_0)$ followed by the passive linear-optic unitary U_I^\dagger efficiently recombines the information-bearing light to one desired output mode, shown as the first mode \hat{b}_1 in Fig. 1. This phase ϕ_H allows optimizing which field quadrature to homodyne to maximize the CFI. If the physical sensor's mathematical description naturally reduces to an array of M MZIs, as in [30], [31] and [32], the conjugate phases $-\vec{\theta}(x_0)$ can be translated to phases applied *after* the MZIs. If little is known about the functions $\vec{\theta}(x)$, i.e., how the scene parameter x is encoded in the M modes, the linear recombination must be determined via an active, potentially adaptive measurement strategy, as discussed in [26, 27, 35].

The $2M$ -mode output state $|\psi_H\rangle$ is a linear optical uni-

tary $U(x)$ applied to the Gaussian input state $|\psi_0\rangle$, where

$$U(x) = U_H U_I^\dagger U_{x_0}^\dagger U_x U_I \quad (5)$$

with $U_I = [F_{2 \times 2} \otimes \mathbb{I}_{M \times M}] [\mathbb{I}_{2 \times 2} \otimes F_{M \times M}] = F_{2 \times 2} \otimes F_{M \times M}$, and $U_x = D(\vec{\theta}(x)) \oplus \mathbb{I}_{M \times M}$, where $D(\vec{\theta}(x))$ is an $M \times M$ diagonal matrix with diagonal elements $\vec{\theta}(x)$, and $U_H = \text{diag}(e^{i\phi_H}, 1, \dots, 1)$. Therefore,

$$U(x) = \frac{1}{2} U_H \left[\begin{pmatrix} 1 & 1 \\ 1 & 1 \end{pmatrix} \otimes F^\dagger (e^{i[\vec{\theta}(x) - \vec{\theta}(x_0)]} \mathbb{I}_{M \times M}) F + \begin{pmatrix} 1 & -1 \\ -1 & 1 \end{pmatrix} \otimes \mathbb{I}_{M \times M} \right], \quad (6)$$

of which two matrix elements will be important:

$$U_{1,1}(x) = \frac{1}{2} e^{i\phi_H} \left[\frac{1}{M} \sum_m^M e^{i[\theta_m(x) - \theta_m(x_0)]} + 1 \right], \quad (7)$$

$$U_{1,M+1}(x) = \frac{1}{2} e^{i\phi_H} \left[\frac{1}{M} \sum_m^M e^{i[\theta_m(x) - \theta_m(x_0)]} - 1 \right]. \quad (8)$$

The statistics of a single-mode, real-quadrature, quantum-noise-limited homodyne measurement are given by mean $d_{H,1}$ and variance $V_{H,1,1}(x)$. Since all the components of U are Gaussian, we track the quadrature mean vector \vec{d}_H and CM V_H of the output state $|\psi_H\rangle$ using $\vec{d}_H(x) = S(x) \vec{d}_0$ and $V_H(x) = S(x) V_0 S^T(x)$, where $S(x)$ can be found from $U(x)$ using Eq. 3. Since the real quadrature of mode \hat{a}_{M+1} is the only input quadrature with non-zero mean, $d_{H,1} = S_{1,M+1}(x) d_{0,1}$, where $S_{1,M+1}(x) = \text{Re}\{U_{1,M+1}(x)\}$. Therefore,

$$d_{H,1}(x) = \frac{1}{2} \left[\frac{1}{M} \sum_m^M \cos(\theta_m(x) - \theta_m(x_0) + \phi_H) - \cos(\phi_H) \right] d_{0,1}. \quad (10)$$

To evolve the CM, we recognize that the quadrature variances of the uncorrelated input modes \hat{a}_m are all equal except for those of mode \hat{a}_1 and write

$$V_H(x) = S(x) \left[\frac{1}{2} \mathbb{I} S^T(x) + \sum_m^{4M} \left(V_{0,1,1} - \frac{1}{2} \right) S^T(x)_{1,m} + \left(V_{0,2M+1,2M+1} - \frac{1}{2} \right) S^T(x)_{2M+1,m} \right], \quad (11)$$

and thus the variance of the measured quadrature is:

$$V_{H,1,1}(x) = \frac{1}{2} \left[1 + (2V_{0,1,1} - 1) S(x)_{1,1}^2 + (2V_{0,2M+1,2M+1} - 1) S(x)_{1,2M+1}^2 \right], \quad (12)$$

where we have used the fact that $S(x)S^T(x) = \mathbb{I}$ for any passive symplectic operator. Using $S(x)_{1,1} = \text{Re}\{U_{1,1}(x)\}$ and $S(x)_{1,2M+1}^2 = \text{Im}\{U_{1,1}(x)\}$ (Eq. 3), the variance becomes

$$\begin{aligned} V_{H,1,1}(x) = & \frac{1}{2} \left[1 + (2V_{0,1,1} - 1) \right. \\ & \left(\frac{1}{M} \sum_m^M \frac{\cos(\theta_m(x) - \theta_m(x_0) + \phi_H)}{2} + \frac{\cos(\phi_H)}{2} \right)^2 \\ & + (2V_{0,2M+1,2M+1} - 1) \\ & \left. \left(\frac{1}{M} \sum_m^M \frac{\sin(\theta_m(x) - \theta_m(x_0) + \phi_H)}{2} + \frac{\sin(\phi_H)}{2} \right)^2 \right] \end{aligned} \quad (13)$$

The classical Fisher information (CFI) for estimating a parameter x from a Gaussian random variable is known to be given by $I_x = I_{x,d} + I_{x,V}$, where

$$I_{x,d} = \frac{1}{V_{H,1,1}(x)} \left(\frac{\partial d_{H,1}(x)}{\partial x} \right)^2 \quad (14)$$

$$I_{x,V} = \frac{1}{2} \left(\frac{1}{V_{H,1,1}(x)} \frac{\partial V_{H,1,1}(x)}{\partial x} \right)^2. \quad (15)$$

In the limiting case $|x - x_0| \ll 1$, the first term is

$$\lim_{x \rightarrow x_0} I_{x,d} = \frac{\langle \partial\theta(x_0) \rangle^2 \sin^2(\phi_H) d_{0,1}^2}{4[V_{0,1,1} \cos^2(\phi_H) + V_{0,2M+1,2M+1} \sin^2(\phi_H)]}. \quad (16)$$

For our input state $|\psi_0\rangle$, $d_{0,1} = \sqrt{2}\alpha$, $V_{0,1,1} = (1/2)e^{2r}$, and $V_{0,2M+1,2M+1} = (1/2)e^{-2r}$, where α is the coherent state amplitude, and r quantifies the squeezing in our single-mode squeezed-vacuum source. Choosing $\phi_H = \pi/2$ to maximize the sensitivity of $d_{H,1}(x)$ to the parameter x , it can be shown that $\lim_{x \rightarrow x_0} I_{x,V} = 0$ and that the CFI has the final expression

$$\lim_{x \rightarrow x_0} I_x = \langle \partial\theta(x) \rangle^2 N_v (\sqrt{N_s} + \sqrt{1 + N_s})^2. \quad (17)$$

Fixing the total photon-unit probe energy $N = N_v + N_s$, the optimal energy allocation is $N_s = N^2/(2N + 1)$. The maximized CFI is $\lim_{x \rightarrow x_0} I_x = \langle \partial\theta(x) \rangle^2 N(N + 1)$, which neatly factors into a prefactor that depends on the phases $\theta_m(x)$ and a probe-dependent component that exhibits Heisenberg scaling with the total probe energy.

RF Signal Estimation with a Photonic Receiver— Our distributed sensing design applies to any situation in which the optical phases acting on a set of orthogonal optical modes are modulated by a signal that depends on one unknown parameter. One example is the estimation of some property of an incident RF field using a large sensor array in an RF photonic receiver antenna, a quantum sensing application for which CV entanglement was recently shown to improve upon classical sensitivity [30]. This work sought to estimate the angle of incidence ϕ

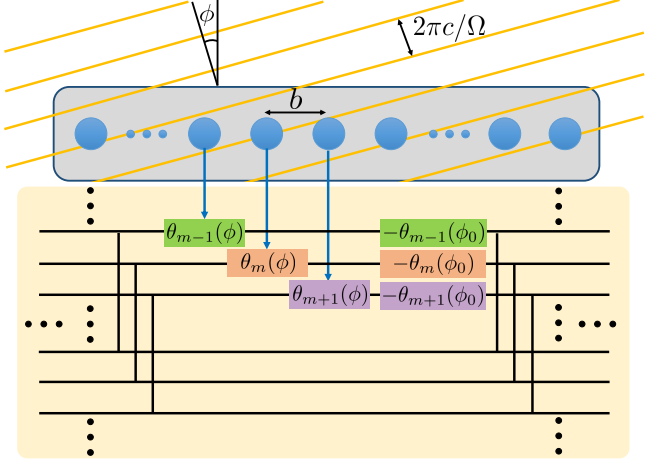


FIG. 2. Application of our entanglement-enhanced sensor framework (Fig. 1) to a 1D phased array of RF-photonic sensors. The angle of incidence ϕ of the RF field (yellow lines) is estimated using RF-amplitude dependent optical phase modulators positioned at lateral positions mb , which modulate one branch of M optical MZIs. Additional unitary transformations before and after the MZIs are excluded here.

from M RF-amplitude dependent optical phase modulators driving phases $\theta_m(\phi)$ on one arm of M optical MZIs (Fig. 2). In this case, the variation in optical phases arises from the spatial distribution of the sensors, which we take to have uniform linear separation b . For freely time-evolving optical field $E_m(t) = E e^{i\omega t + \theta_0 + \theta_m(\phi)}$ with amplitude E , optical frequency ω , and phase offset θ_0 , the position-dependent RF-modulated phase is [30]

$$\theta_m(\phi) = A \sin \left(\Omega \left(t + \frac{mb \sin(\phi)}{c} \right) \right), \quad (18)$$

where A is the RF-photonic amplitude-phase modulation strength, Ω is the monochromatic RF frequency, mb gives the relative position of the m^{th} sensor, and $c = 3e8$ m/s is the speed of light. Eq. 18 can be used to compute the prefactor terms $\langle \partial\theta(\phi) \rangle$ and $\langle \partial\theta(\phi)^2 \rangle$ in the QFI and CFI calculations, in Eqs. 4 and 17, respectively.

For an entangled probe in the high energy limit, the maximum QFI (Eq. 4) for the angle-of-incidence estimation task will exhibit exhibiting $H_\phi \propto 2N^2$, which is achieved by setting $N_s = N$, i.e., giving all of the probe energy to the single-mode SV [28]. Our sensor design can fully saturate the QFI in the high probe energy limit by allocating $N_s = N$ and by applying the quadrature rotation $\phi_H = (1/2) \cos^{-1}(-2\sqrt{N_s(1 + N_s)}/(1 + 2N_s))$, which achieves $I_\phi \propto 2N^2$. However, using our probe that uses both coherent and SV states, with $N_s = N^2/(2N + 1)$ and $\phi_H = \pi/2$ retains Heisenberg scaling with energy for the sensitivity, with a CFI $I_\phi \propto N^2$ that falls just a factor of two short of the fully optimized QFI. This price in sensitivity is balanced by a more feasible experimental system featuring at most half the

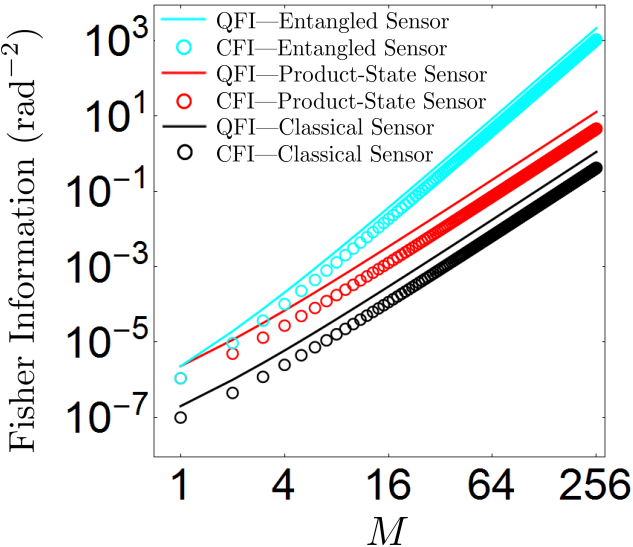


FIG. 3. QFI (solid lines) and CFI (open circles) for our entanglement-enhanced sensor design (Fig. 1), a similar design with product-state SV injected into each MZI, and a classical sensor with only coherent states, where $A = 0.1$, $\Omega = 30\text{kHz}$, $b = 10m$, and $N = 10M$.

squeezed-light energy, which is easily replaced by a laser, and a fixed homodyne quadrature that removes the concern that intensity fluctuations in the pump laser will negatively influence the homodyne sensitivity [27].

In Fig. 3, we plot the QFI and CFI for sensing a near-normal incident ($|\phi| \ll 1$) RF signal under the condition that the total probe energy budget N scales with the size of the sensor array M . In this case, the Heisenberg scaling $I_\phi = O(N^2)$ with probe energy translates into Heisenberg scaling $I_\phi = O(M^2)$ with the number of phase modulators being driven by the RF field. This scaling advantage is not accessed by M individual quantum sensors probing each phase, as both a classical sensor that distributes only coherent states to the M interferometers and a sensor that injects independent, product-state SV into each MZI exhibit $H_\phi = O(M)$ and $I_\phi = O(M)$ (Fig. 3). Our entanglement enhanced scheme enables a potentially large advantage over non-entangled designs for large RF sensor arrays.

Other Photonic Sensing Examples— Our powerful general framework allows us to accurately analyze previously studied quantum-enhanced sensing applications in terms of a simple M MZI sensor network. One such example is the use of entanglement across free-space optical modes with a single physical sensor to estimate a small lateral displacement δ of an optical beam [32], for example to perform quantum-enhanced atomic force microscopy (AFM). In this example, the input modes \hat{a}_m are a set of $2M$ spatially co-localized, mutually orthogonal optical modes (e.g., Hermite-Gauss modes for a Gaussian apodized probe aperture) with negligible loss in the near

field regime. A small lateral displacement ($\delta \ll 1$) affects these spatial modes differently, with the effects on modal energy crosstalk quantified by a nearest-neighbor overlap matrix Γ . These mode interactions can be unitarily converted into a set of M MZIs with linearly δ -dependent phases $2\lambda_m\delta$, where the λ_m depend on the eigenvalues of Γ . We can then apply the entangled sensor framework reported here and find a CFI given by Eq. 17, where the prefactor becomes $\langle \partial\theta(x) \rangle^2 = (1/M^2)(\sum_{m=1}^M 2\lambda_m)^2$. Notably, since $\sum_{m=1}^M \lambda_m \propto M^{3/2}$ [32], our analysis recovers the M -dependence of the CFI prefactor, which arises because the crosstalk between spatial modes becomes more and more sensitive to small lateral as the mode order m increases [32]. Our framework independently achieves the factor of M improvement over the Heisenberg scaling $I_\delta = O(N^2)$, the optimal scaling for this sensing task.

Our sensor framework is also equipped to describe temporally entangled optical probes and dynamic physical systems. For example, consider the estimation of the thermal conductivity k of a slab of uniform, isotropic dielectric material, in which one branch of an optical fiber MZI is embedded at lateral position $y = y_0$. If the slab is heated to an initial distribution $u(y, 0)$ and allowed to relax to a steady state, the k -dependent phase induced by the temperature $u(y_0, t)$ could be probed at times $t = m/W$, where W is the optical source bandwidth and the number of orthogonal temporal modes $M = WT$ is given by the time-bandwidth product. Following our sensor framework, the M temporal modes of a CV entangled state could be sequentially injected into the fiber MZI along with a coherent state. The functional form $\theta_m(k)$ of the M phases will depend on the solution to the heat equation $\partial u(y, t)/\partial t = (k/\rho c_p)\partial^2 u(y, t)/\partial y^2$, where ρ is the material density and c_p is its specific heat, as well as the temperature-dependent Sellmeier equation for the optical refractive index of the fiber material. Even so, as long as the first derivatives of $\theta_m(k)$ can be computed analytically or numerically, Eq. 17 can be used to evaluate the CFI and bound the variance of any unbiased estimator of k using our entangled sensor design. Assuming constant power sources, distributed sensing across temporal modes naturally leads to a total photon-unit energy N that scales linearly with M . The Heisenberg scaling $I_k = O(N^2)$ will therefore readily extend to $I_k = O(M^2)$, and a significant advantage from entanglement across the integration time T can be expected.

Discussion—Several photonic sensing tasks can be reduced to estimating a scalar parameter x that modulates phases $\theta_m(x)$, $1 \leq m \leq M$, e.g., in M Mach-Zehnder Interferometers (MZIs). The examples we discussed include passive sensors, e.g., sensor pixels in an RF photonic antenna phase modulated by an impinging RF signal, read out optically within the receiver; as well as active sensors, e.g., a multimode optical probe used to sense a small displacement of a nano-cantilever in an atomic-force micro-

scope. We discussed some other applications that reduce to the aforesaid abstract scenario, and several that we did not such as quantum process verification for photonic quantum circuits, and quantum network tomography.

We proved a Heisenberg limited scaling of the Fisher Information $I_x = O(N^2)$ in estimating the parameter in terms of the total photon-unit energy N employed by the sensor. Furthermore, we argued that under certain circumstances as discussed in the examples treated in the paper, we see Heisenberg scaling in M as well, i.e., $I_x = O(M^2)$. The latter effect, which we showed is true for two examples we studied, is especially significant when M is large.

There are several avenues to get constant factor improvement in I_x over our simple receiver design, e.g., by optimizing the recombination unitary U_I^\dagger for a priori known functions $\vec{\theta}(x)$, or adaptively tuning it when limited information is available about them. This will involve arbitrary tuning of $\mathcal{O}(M^2)$ phases in a programmable linear-optic circuit [36, 37], each of which may need to be controlled in nontrivial ways in response to nuisance parameters within the functions $\vec{\theta}(x)$ in order to maintain optimality. When optical loss and noise is included in our analysis, the Heisenberg scalings (with respect to N and M) will both go away, and $I_x = O(MN)$ will prevail. However, there will be a constant factor improvement in I_x over a classical sensor in the long integration time limit, which can be significant (e.g., an order of magnitude or more) if the losses are moderate, and if M is large, as reported for the problem studied in [12]. We leave a detailed analysis of our problem with loss and noise, along similar lines, and quantitative applications of it to more real-life photonic (and non-photonic) quantum estimation problems, for future work.

Acknowledgement—This research was supported by the Office of Naval Research, contract number: N00014-19-1-2189. The authors acknowledge valuable discussions with Quntao Zhuang, Zheshen Zhang, and Linran Fan. MRG and CNG contributed equally to this work.

-
- [1] E. T. Khabiboulline, J. Borregaard, K. De Greve, and M. D. Lukin, Phys. Rev. Lett. **123**, 070504 (2019).
- [2] D. E. Bruschi, A. Datta, R. Ursin, T. C. Ralph, and I. Fuentes, Phys. Rev. D **90**, 124001 (2014).
- [3] D. Branford, H. Miao, and A. Datta, Phys. Rev. Lett. **121**, 110505 (2018).
- [4] B. P. Abbott *et al.* (LIGO Scientific Collaboration and Virgo Collaboration), Phys. Rev. Lett. **116**, 061102 (2016).
- [5] B. P. Abbott *et al.* (LIGO Scientific Collaboration and Virgo Collaboration), Phys. Rev. Lett. **119**, 161101 (2017).
- [6] D. Branford, C. N. Gagatsos, J. Grover, A. J. Hickey, and A. Datta, Phys. Rev. A **100**, 022129 (2019).
- [7] E. Bisketzi, D. Branford, and A. Datta, New Journal of Physics **21**, 123032 (2019).
- [8] P. C. Humphreys, M. Barbieri, A. Datta, and I. A. Walmsley, Phys. Rev. Lett. **111**, 070403 (2013).
- [9] C. N. Gagatsos, D. Branford, and A. Datta, Phys. Rev. A **94**, 042342 (2016).
- [10] P. A. Knott, T. J. Proctor, A. J. Hayes, J. F. Ralph, P. Kok, and J. A. Dunningham, Phys. Rev. A **94**, 062312 (2016).
- [11] T. J. Proctor, P. A. Knott, and J. A. Dunningham, Phys. Rev. Lett. **120**, 080501 (2018).
- [12] Q. Zhuang, Z. Zhang, and J. H. Shapiro, Phys. Rev. A **97**, 032329 (2018).
- [13] C. Weedbrook, S. Pirandola, R. García-Patrón, N. J. Cerf, T. C. Ralph, J. H. Shapiro, and S. Lloyd, Rev. Mod. Phys. **84**, 621 (2012).
- [14] A. Ferraro, S. Olivares, and M. G. Paris, arXiv preprint quant-ph/0503237 (2005).
- [15] M. Chen, N. C. Menicucci, and O. Pfister, Phys. Rev. Lett. **112**, 120505 (2014).
- [16] N. Takanashi, W. Inokuchi, T. Serikawa, and A. Furusawa, Opt. Express **27**, 18900 (2019).
- [17] S. D. Bartlett, B. C. Sanders, S. L. Braunstein, and K. Nemoto, Phys. Rev. Lett. **88**, 097904 (2002).
- [18] J. Eisert, S. Scheel, and M. B. Plenio, Phys. Rev. Lett. **89**, 137903 (2002).
- [19] J. Fiurásek, Phys. Rev. Lett. **89**, 137904 (2002).
- [20] G. Giedke and J. Ignacio Cirac, Phys. Rev. A **66**, 032316 (2002).
- [21] N. J. Cerf, O. Krüger, P. Navez, R. F. Werner, and M. M. Wolf, Phys. Rev. Lett. **95**, 070501 (2005).
- [22] M. Takeoka and M. Sasaki, Phys. Rev. A **78**, 022320 (2008).
- [23] C. Wittmann, U. L. Andersen, M. Takeoka, D. Sych, and G. Leuchs, Phys. Rev. Lett. **104**, 100505 (2010).
- [24] J. Niset, J. Fiurásek, and N. J. Cerf, Phys. Rev. Lett. **102**, 120501 (2009).
- [25] M. Takeoka and S. Guha, Phys. Rev. A **89**, 042309 (2014).
- [26] G. Gramegna, D. Triggiani, P. Facchi, F. A. Narducci, and V. Tamma, arXiv preprint arXiv:2003.12550 (2020).
- [27] G. Gramegna, D. Triggiani, P. Facchi, F. A. Narducci, and V. Tamma, arXiv preprint arXiv:2003.12551 (2020).
- [28] T. Matsubara, P. Facchi, V. Giovannetti, and K. Yuasa, New Journal of Physics **21**, 033014 (2019).
- [29] While writing this paper, we came across two concurrent recent papers from the same set of authors that analyzed a model closely related to ours [26, 27]. Our paper differs from, and complements these papers in the following ways. We calculate the quantum Fisher Information (QFI) to evaluate the fundamental limit of sensitivity attainable with *any* receiver design. Further, our optical probe is different than theirs in that it includes a strong coherent-state (laser-light) source, so that the entangled squeezed light only contributes to a small portion of the total mean photon number budget, unlike theirs where the squeezed light contributes to *all* the probe power, and hence must have much more squeezing to achieve a given performance which would be harder to generate. Finally, we do not use an adaptive measurement (such as the one in [28]) since we assume our scene parameter x is very close to a pre-estimate x_0 , i.e., $|x - x_0| \ll 1$. The choices in our model as described above, were based on the practical photonic sensors described in the Introduction, and with experimental feasibility of implementation in mind.

- Finally, as a side note, our paper develops the rigorous theory behind a recent experimental demonstration by our colleagues at University of Arizona [30], paving the way for future, more scalable, experimentation.
- [30] Y. Xia, W. Li, W. Clark, D. Hart, Q. Zhuang, and Z. Zhang, arXiv preprint:1910.08825 (2019), (To be published in *Phys. Rev. Lett.*).
- [31] M. R. Grace, C. N. Gagatsos, Q. Zhuang, and S. Guha, (2020), arXiv:2003.12545 [quant-ph].
- [32] H. Qi, K. Brádler, C. Weedbrook, and S. Guha, arXiv preprint arXiv:1808.01302 (2018).
- [33] S. Pirandola, B. R. Bardhan, T. Gehring, C. Weedbrook, and S. Lloyd, *Nat. Photonics* **12**, 724 (2018).
- [34] S. L. Braunstein and C. M. Caves, *Phys. Rev. Lett.* **72**, 3439 (1994).
- [35] Q. Zhuang and Z. Zhang, *Phys. Rev. X* **9**, 041023 (2019).
- [36] M. Reck, A. Zeilinger, H. J. Bernstein, and P. Bertani, *Phys. Rev. Lett.* **73**, 58 (1994).
- [37] W. R. Clements, P. C. Humphreys, B. J. Metcalf, W. Steven Kolthammer, and I. A. Walmsley, *Optica*, *OPTICA* **3**, 1460 (2016).